# Analysis and Shape Inequalities for Gas-Solid Reactions with Changing Volume

**Giacomo Cao, William Strieder, and Arvind Varma**
Dept. of Chemical Engineering, University of Notre Dame, Notre Dame, IN 46556

*For gas-solid noncatalytic reactions following the sharp-interface model, some fundamental aspects, not discussed previously in the literature, are presented for particle shapes where diffusion processes are described by a single space dimension. A detailed structure analysis of the solution for monotone nonlinear kinetics reveals interesting differences in the dynamics of the interfacial reaction front, including local maxima and minima in the rate of reaction interface motion, depending on particle shape and expanding or shrinking particle size. Rigorous shape inequalities on the interfacial reactant concentration, the motion of the reaction front and the particle conversion for the sphere and slab, and cylinder and slab geometries are obtained for any nonlinear monotonically increasing reaction kinetics and a wide range of parameter values. By taking advantage of these inequalities, the fraction of original solids of spherical or cylindrical shape, which remains unconverted at the exit of a fluidized-bed reactor, is bounded by the corresponding quantities related to the slab shape. As an example, a first-order reaction of the gaseous reactant is considered, where expressions for the reactor are obtained analytically, without any assumptions about possible controlling regimes. These analytical bounds for reactor conversion closely approximate the numerical solutions for design purposes.*

## Introduction

In the context of gas-solid noncatalytic reactions, several models have been developed (cf. Szekely et al., 1976; Doraiswamy and Sharma, 1984 for comprehensive reviews). This work focuses on the sharp interface model (SIM), which is applicable to relatively nonporous solid reactants. The reaction is assumed to occur at a sharp interface between the product layer and the unreacted core of the solid consumed as the reaction proceeds. Despite its simplicity, the SIM can be used to describe, once incorporated into a suitable reactor model, a variety of chemical and metallurgical processes including the roasting of zinc sulfide (Yoshida and Wen, 1970) and the combustion of coal (Baron et al., 1978). For isothermal conditions, equimolar counterdiffusion of reacting and product gases, and pseudo-steady-state approximation, new features of the SIM have been uncovered (Cao et al., 1993) by analyzing the structure of the solution as the reaction evolves in time for spherical particles of unchanging size. An *a priori* description of the reaction process, which is independent of the kinetic law with respect to the gaseous reactant, was obtained. In particular, we demonstrated that the gaseous reactant concentration at the reaction interface reaches the bulk value at the cessation of the reaction, either increasing monotonically or going through a minimum, depending on the extent of the external mass-transfer resistance. It is worth noting that the resulting physical insight permitted us to develop a strategy for obtaining rather good approximate analytical solutions for the time to reach a desired conversion of the solid reactant for several nonlinear monotonically increasing kinetics with respect to the gaseous reactant.

If the volume of product formed differs from that of the solid reactant, the particle size changes as the reaction occurs. In particular, the particle expands (or shrinks) in size if the volume of product formed is larger (or smaller) than that of the solid reactant. A number of examples of noncatalytic gas-solid reactions following the SIM with particles of changing size have been reported (cf. Levenspiel, 1972). This work extends the analysis of the qualitative behavior of gas-solid noncatalytic reactions following the SIM, developed in our previous

Correspondence concerning this article should be addressed to either W. Strieder or A. Varma.
G. Cao is on leave from Dipartimento di Ingegneria Chimica e Materiali, Universita' di Cagliari, Piazza d'Armi, 09123 Cagliari, Italy.

study (Cao et al., 1993) for spherical particles of fixed size, to the case of one-dimensional geometries, that is, slab, cylindrical and spherical particles of *changing size*. Mazet (1992) presented some considerations for the effect of particle geometry, as well as the ratio of the product and reactant densities for the case of SIM. Although some interesting comments were made on the rate of advance of the reaction front in various controlling regimes, only the first-order reaction of the gaseous reactant was treated, and it was claimed that a systematic study was not feasible for kinetics of arbitrary order. This article shows that for *any* nonlinear monotonically increasing kinetics, a systematic analysis of the evolution of the reaction as a function of the physicochemical parameters is possible, and this allows us to establish rigorously the effect of particle geometry for both fixed and changing sizes.

Depending on the relative magnitudes of external mass transfer and internal product layer diffusional resistances, dynamics of the interfacial reaction front are uncovered. Rigorous shape inequalities on the interfacial reactant concentration, motion of the reactant front and particle conversion for the shape and the slab, and the cylinder and the slab combinations are obtained for any monotone nonlinear kinetics and volume change. By taking advantage of this *a priori* information, it is demonstrated that the fraction of original solids of either spherical or cylindrical shape which remains unconverted at the exit of a fluidized-bed reactor, is bounded by the corresponding quantities for particles of slab shape.

For a first-order reaction, by comparing the analytical bounding expression to numerical computations, it is shown that this bound on the mean conversion of the solids leaving the reactor is a good measure of the true value and can be used easily for design purposes for constant volume, shrinking or expanding particles.

## Basic Equations

In this section, we present the governing equations for an isothermal nonlinear noncatalytic reaction occurring in a one-dimensional slab, cylindrical or spherical particle of initial characteristic size $R_0$ between a gas $A$ and a solid $B$, according to the general scheme:

$$\nu_A A_{(g)} + \nu_B B_{(s)} \rightarrow \nu_P P_{(g)} + \nu_S S_{(s)}.$$

The reaction is assumed to occur at a sharp interface between the exhausted outer shell and the unreacted core of the solid, that is, the SIM holds. In addition, equimolal counterdiffusion of gaseous reactants and products is assumed, and the pseudo-steady-state approximation is made. To include various particle shapes in the analysis and yet account for solid volume change during reaction, the characteristic initial value $R_0$, particle size $R$, and interface $R_i$ coordinates are defined, where $R$ represents the slab half-thickness, and the cylinder and sphere radius. To illustrate the change of volume during reaction, the case of a sphere is shown in Figure 1. By considering the moles of $B$ reacted and moles of $S$ created, together with the reaction stoichiometry, the following relationship can be obtained:

$$R = R_0 \left\{ \frac{\rho_B \nu_S M_S}{\rho_S \nu_B M_B} + \left(1 - \frac{\rho_B \nu_S M_S}{\rho_S \nu_B M_B}\right) \left(\frac{R_i}{R_0}\right)^{F_P} \right\}^{1/F_P} \tag{1}$$

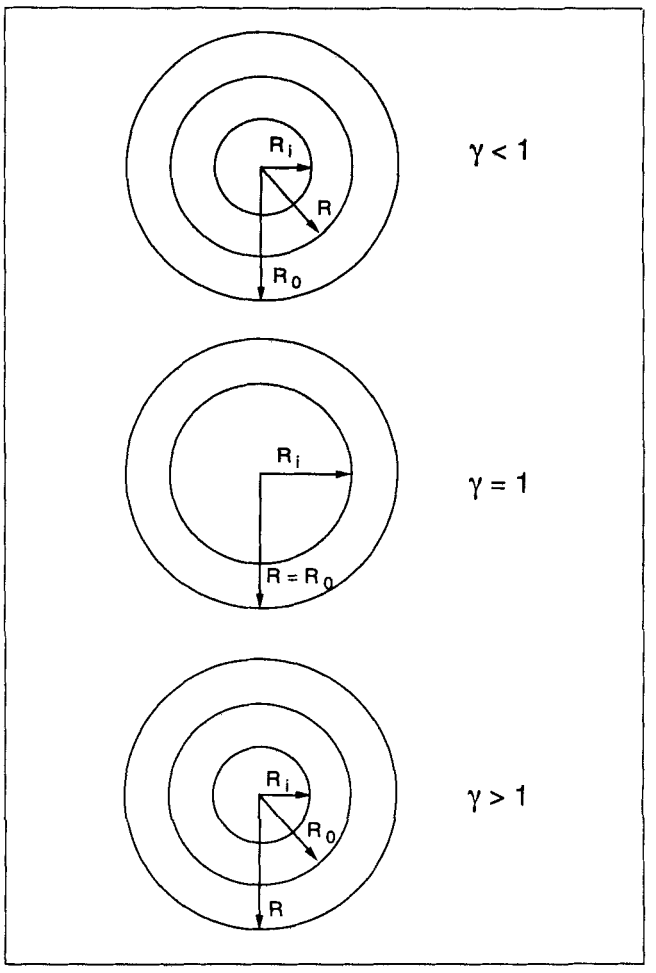


**Figure 1. Sharp interface model for a sphere for shrinking ($\gamma < 1$), constant volume ($\gamma = 1$) and expanding ($\gamma > 1$) particles.**

where $F_P = 1$ for slab, 2 for cylindrical, and 3 for spherical particles, respectively.

Diffusion of the reactant gas through the external film around the particle and through the product layer are the resistive steps involved before the reaction occurs. The rate of the former can be written as

$$R_A = S_p k_{g0} (R/R_0)^{-n} (C_{Ab} - C_{As}) \tag{2}$$

where $S_p$ represents the particle surface area at any time. The film mass-transfer coefficient for the case of particles with changing size can be related to the corresponding value $k_{g0}$ if the particle had remained of constant size (cf. Carberry, 1976), through the ratio of the change in particle dimension ($R/R_0$), and a positive parameter $n$ that depends on the particle Reynolds number. The expressions for the diffusion rate through the product layer can be derived easily for any particle geometry and are given as follows:

$$R_A = S_p D_e \frac{C_{As} - C_{Ai}}{R - R_i}, \qquad F_p = 1 \tag{3}$$

$$R_A = S_p D_e \frac{C_{As} - C_{Ai}}{R \ln (R/R_i)}, \qquad F_p = 2 \tag{4}$$

$$R_A = S_p D_e \frac{C_{As} - C_{Ai}}{(R - R_i)(R/R_i)}, \quad F_p = 3 \tag{5}$$

for a slab, cylindrical and spherical particle, respectively. The rate of chemical reaction at the interface can be expressed in the general form

$$R_A = S_{pi} f(C_{Ai}) \tag{6}$$

where $f(C_{Ai})$ is *any* nonlinear monotonically increasing function, and $S_{pi}$ is the surface area of the unreacted core. The material balance for the solid reactant $B$ in terms of movement of the reaction interface is given by

$$-\frac{d}{dt}\left(V_{pi}\frac{\rho_B}{M_B}\right) = \frac{\nu_B}{\nu_A} R_A \tag{7}$$

with initial condition

$$R = R_i = R_0; \quad t = 0. \tag{8}$$

Introducing the dimensionless quantities

$$u_s = \frac{C_{As}}{C_{Ab}}, \quad u_i = \frac{C_{Ai}}{C_{Ab}}, \quad Bi = \frac{k_{g0} R_0}{D_e},$$

$$z = \frac{R_i}{R_0}, \quad \psi_A = \frac{R_A}{S_{p0} f(C_{Ab})}, \quad \tau = \frac{\nu_B f(C_{Ab}) M_B t}{\nu_A \rho_B R_0},$$

$$Da = \frac{f(C_{Ab}) R_0}{D_e C_{Ab}}, \quad \gamma = \frac{\rho_B \nu_S M_S}{\rho_S \nu_B M_B}, \tag{9}$$

Equations 1-8 reduce to their dimensionless forms

$$\alpha = [\gamma + (1 - \gamma) z^{F_p}] \tag{10}$$

$$\psi_A = \frac{Bi(1 - u_s)}{Da} \alpha^{(F_p - 1 - n)/F_p} \tag{11}$$

$$\psi_A = \frac{(u_s - u_i)}{Da} q[\alpha(z), z] \tag{12}$$

$$g(u_i) = \psi_A / z^{(F_p - 1)} \tag{13}$$

$$-\frac{dz}{d\tau} = g(u_i) \tag{14}$$

$$z = 1, \quad \tau = 0, \tag{15}$$

where the function $q[\alpha(z), z]$ is related to particle geometry as follows:

$$q[\alpha(z), z] = (\alpha - z)^{-1}, \qquad F_p = 1 \tag{16}$$

$$q[\alpha(z), z] = [\ln(\alpha^{1/2}/z)]^{-1}, \quad F_p = 2 \tag{17}$$

$$q[\alpha(z), z] = \frac{z\alpha^{1/3}}{(\alpha^{1/3} - z)}, \qquad F_p = 3. \tag{18}$$

The solution of the problem given by coupling Eqs. 10-18 provides the dimensionless position of the reaction interface, $z$ which is related to the solid conversion, $X$ through

$$X = 1 - z^{F_p} \tag{19}$$

as a function of time, $\tau$. Analytical solutions of this problem can be found by combining Eqs. 10-13 and 16-18 and substituting the obtained kinetic expression into Eq. 14, *only* if $g(u_i)$ is a linear function. In such a case the problem can be solved for $\tau$ as a function of $z$ (or $X$) in a straightforward manner (cf. Carberry, 1976; Doraiswamy and Sharma, 1984). Rather good approximate analytical solutions to this problem for nonlinear monotone kinetics, $g(u_i)$, were obtained recently (Cao et al., 1993).

## Analysis of Reaction Behavior

One aim of this work is to examine the structure of the solution as the reaction evolves in time, starting with zero solid conversion ($z = 1$), going eventually to completion ($z = 0$), to obtain *a priori* information about the reaction progress. For this, note that coupling Eqs. 10-13 and 16-18 gives

$$f_{F_p}(z) \equiv z^{(F_p - 1)}[Bi\{q[\alpha(z), z]\}^{-1} + \{\alpha^{(F_p - 1 - n)/F_p}\}^{-1}]$$

$$= \frac{Bi(1 - u_i)}{Da\, g(u_i)} \equiv h(u_i). \tag{20}$$

It should be clear that the nature of functions $f_{F_p}$ and $h$ governs the exact evolution of the reaction in time. The function $f$ contains the effects of particle shape ($F_p$), volume expansion ($\gamma$), and the interplay between the external mass transfer and product layer diffusion ($Bi$ and $n$). As we shall see, depending on the numerical values of these parameters, $f_{F_p}$ exhibits some subtle and unusual features.

For the rate functions, $g(u_i)$ is monotone increasing [$g'(u_i) \geq 0$]. For such $g$, $h' \leq 0$: $h$ decreases as $u_i$ increases. As is usually done (Doraiswamy and Sharma, 1984; Mazet, 1992), the analysis for the sphere and cylindrical particle geometries will be performed for the low Reynolds number, where $n = 1$. This assignment of $n$ is appropriate for the large class of fluidized "areatable" particles as defined in Geldart's diagram (Geldart, 1986). For the slab, the $n = 0$ case is also discussed, but the corresponding results are reported in the Appendix.

The case of two different particle geometries is detailed: the slab ($F_p = 1$) and sphere ($F_p = 3$), since the arguments for cylindrical particles ($F_p = 2$) are similar to those for spherical ones. The engineering justification of the flat plate geometry comes from its simple representation of the limited penetration case even in more complex geometries, as well as its ability to generate shape-independent bounds. In the context of the former, the increase in the external film mass-transfer coefficient $k_{g0}$ for shrinking particles ($\gamma < 1$) suggests that $n = 1$ be considered but for the flat plate $n = 0$ is also of interest. Moreover, it not only allows for simpler analytical derivations but also provides somewhat better bounds for $\gamma > 1$, as will be described later. The mathematical analysis is augmented by the use of a number of illustrations (Figures 2 and 3).

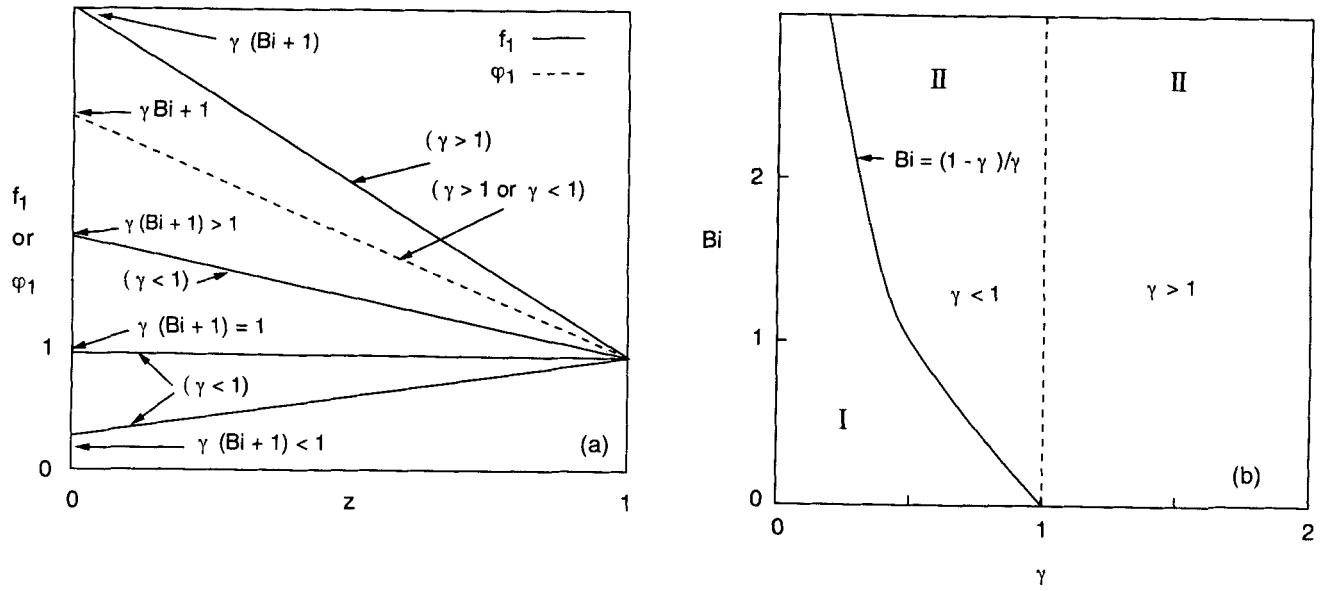


**Figure 2. Slab particles ($F_p = 1$).**

a) Shape of $f_1$ and $\varphi_1$ curves; b) classification of regions in the $Bi$-$\gamma$ plane.

### *Slab particles:* $F_p = 1$

From Eq. 20, for particles of slab shape and $n = 1$, we have

$$f_1(z) = \gamma(Bi+1) - \gamma(Bi+1)z + z = h(u_i) \qquad (21)$$

It follows from Eqs. 20 and 21 that there exists a unique value of $z$ for any given $u_i$. Figure 2a displays the straight lines $f_1$ of Eq. 21 vs. the interface coordinate $z$, with slope $f_1' = 1 - \gamma(Bi+1)$ for various combinations of the parameters $\gamma$ and $Bi$. For a shrinking particle ($\gamma < 1$), the three lowest lines in Figure 2a are obtained for $Bi$ increasing from zero. By setting $f_1' = 0$, it follows that $Bi = (1-\gamma)/\gamma$, which allows us to define the regions in Figure 2b. Region I corresponds to the case where $\gamma < 1$ and $Bi < (1-\gamma)/\gamma$. In this case, as $z$ varies from 1 to 0 (zero solid conversion to reaction completion), $f_1(z)$ decreases monotonically from $f_1(1) = 1$ to $f_1(0) = \gamma(Bi+1) < 1$, as shown by the lowest line of Figure 2a. On the other hand, region II corresponds to the case where $Bi > (1-\gamma)/\gamma$, which implies that $f_1(z)$ increases monotonically from $f_1(1) = 1$ to $f_1(0) = \gamma(Bi+1) > 1$, as shown by the middle line of Figure 2a.

Accordingly, from the righthand side of Eq. 20, the reaction starts at a value of $u_i = u_{i,0}$ given by the unique solution of $h(u_i) = f_1(1) \equiv 1$ and goes to completion at a value of $u_i = u_{if}$ given by the unique solution of $h(u_i) = f_1(0) \equiv \gamma(1+Bi)$ by following the curve $f_1(z)$. As $z$ varies from 1 to 0, the corresponding value of the interface gas concentration, $u_i$ is obtained from the solution of $h(u_i) = f_1(z)$, as given by Eq. 21. It follows then for a shrinking ($\gamma < 1$) slab with $n = 1$ that as the reaction proceeds, $u_i$ increases or decreases monotonically from $u_{i,0}$ to $u_{if}$, if the parameters $Bi$ and $\gamma$ lie in region I or II in Figure 2b for $\gamma < 1$, respectively. Figure 2b for $\gamma > 1$ depicts region II to include the entire area above the $\gamma$ axis.

In physical terms, the behavior can be understood as follows. For $\gamma > 1$, the particle size dimension ($R$), the product layer thickness, and the external mass-transfer resistance from Eq. 2 *all* increase as the reaction proceeds. Thus the interfacial reactant concentration, $u_i$ decreases, resulting in increased $h(u_i)$ and hence $f_1(z)$ following Eq. 20. For this reason, with the progress of reaction, that is, the reacting interface $z$ decreasing, the function $f_1(z)$ increases as observed in Figure 2a. On the other hand, for $\gamma < 1$, both particle size and reaction interface dimensions decrease as the reaction proceeds. Following Eq. 2, now the external mass-transfer resistance decreases while the product layer resistance always increases. Hence the magnitude of the Biot number, $Bi$, governs which resistance dominates. For smaller $Bi$, the external resistance is the stronger, so $u_i$ increases and $f_1$ get smaller as $z$ goes from 1 to 0. The reverse occurs for larger $Bi$, and the crossover is shown geometrically in Figures 2a and 2b.

### *Spherical particles:* $F_p = 3$

In this case, Eq. 20 becomes

$$f_3(z) \equiv (Bi-1)z\{1 - z[(1-\gamma)z^3 + \gamma]^{-1/3}\} + z \equiv h(u_i), \qquad (22)$$

whose behavior is again determined by the relative magnitudes of $\gamma$ and $Bi$. It is apparent that Eq. 22 may admit multiple solutions for a given $u_i$. Since $f_3(1) = 1$ and $f_3(0) = 0$, and $f_3(z) > 0$ as $z$ varies from 1 to 0, this can be demonstrated by considering the expressions of the first and second derivatives of Eq. 22, which can be written as:

$$f_3'(z) = (Bi-1)\left\{1 - \frac{(1-\gamma)z^4 + 2\gamma z}{[(1-\gamma)z^3 + \gamma]^{4/3}}\right\} + 1 \qquad (23)$$

$$f_3''(z) = (Bi-1)(2\gamma)[(1-\gamma)z^3 - \gamma][(1-\gamma)z^3 + \gamma]^{-7/3}. \qquad (24)$$

Note that $f_3'(0) = Bi$ is always positive, while $f_3'(1) = 1 - \gamma(Bi-1)$ changes sign from positive to negative as $Bi$ increases across $Bi = 1 + \gamma^{-1}$ for any positive volume ratio $\gamma$. Since for all $\gamma > 0.5$, the second derivative, $f_3''$ is always positive below ($f_3'' > 0$ for $Bi < 1$, $\gamma > 0.5$) and negative above ($f_3'' < 0$

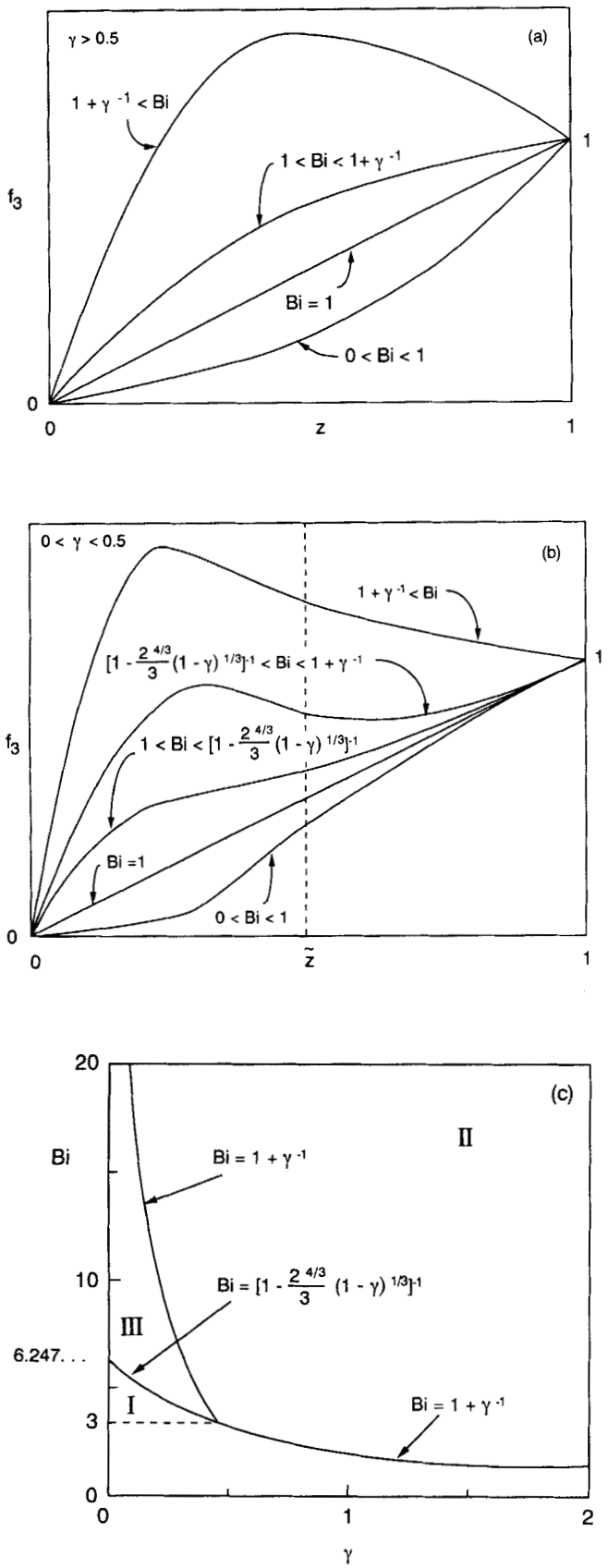


**Figure 3. Spherical particles ($F_p = 3$).**

a) Shape of $f_3$ curves, $\gamma > 0.5$; b) shape of $F_3$ curves, $0 < \gamma < 0.5$; and c) classification of regions in the $Bi$-$\gamma$ plane.

for $Bi > 1$, $\gamma > 0.5$) the unit value of $Bi$, the plot of $f_3$ vs. the reaction coordinate, $z$ can be constructed easily. The curves in Figure 3a are labeled from the bottom to the top for increasing $Bi$. For $Bi = 1$, $f_3$ is a straight line of unit slope. For $Bi < 1 + \gamma^{-1}$, the slope of $f_3$ is positive at both ends, and from either $f_3'' > 0$ for $0 < Bi < 1$ or $f_3'' < 0$ for $1 < Bi < 1 + \gamma^{-1}$, no extremum in $f_3$ can exist. For $Bi > 1 + \gamma^{-1}$, the slope of $f_3$ at $z = 1$ becomes negative and $f_3'' < 0$, so a single maximum in $f_3$ above the value of unity must occur. In the $Bi$-$\gamma$ plane (Figure 3c) for a sphere, the single maximum region is labeled II and the region with no extremum is labeled I.

In the remaining part of the interval, $0 < \gamma < 0.5$, from Eq. 24 $f_3''$ has a single zero $f_3''(\tilde{z}) = 0$ at the inflection point

$$\tilde{z} = [\gamma/(1-\gamma)]^{1/3} \tag{25}$$

The second derivative goes from positive to negative for $Bi < 1$ and negative to positive for $Bi > 1$, as $z$ varies from 0 to 1. Again the case $Bi = 1$ is a straight line of unit slope as shown in Figure 3b. The behavior of $f_3$ depends on the sign of the slope at the inflection point $f'(\tilde{z})$, from Eqs. 22 and 25

$$f_3'(\tilde{z}) = (Bi - 1)\{1 - 3/[2^{4/3}(1-\gamma)^{1/3}]\} + 1, \tag{26}$$

and with increasing Biot number, $f_3'(\tilde{z})$ crosses from positive to negative when $f_3'(\tilde{z}) = 0$

$$Bi = [1 - 2^{4/3}(1-\gamma)^{1/3}/3]^{-1}. \tag{27}$$

In Figure 3b, for the lowest three curves for $0 < Bi < [1 - 2^{4/3}(1-\gamma)^{1/3}/3]^{-1}$, all three derivatives $f_3'(0)$, $f_3'(\tilde{z})$, and $f_3'(1)$ are positive and no relative extremum exists. Once the inflection point derivative changes sign, $f_3'(\tilde{z}) < 0$, and a local maximum must exist between 0 and $\tilde{z}$, as $f_3'(1)$ remains positive. Finally, in the uppermost curve of Figure 3b, both $f_3'(\tilde{z})$ and $f_3'(1)$ are negative, and a global maximum in $f_3$ above unity is observed. In Figure 3c for $0 < \gamma < 0.5$, the lowest three curves generate below $Bi = [1 - 2^{4/3}(1-\gamma)^{1/3}/3]^{-1}$ region I of no extremum, above this $Bi$ up to $1 + \gamma^{-1}$ in region III, two local extrema—a maximum and a minimum—exist on either side of $\tilde{z}$ and above $1 + \gamma^{-1}$ as before we encounter the single maximum region II.

Features of Figures 3a and 3b provide insight into the competing transport processes and role of the Biot number, $Bi$. For $\gamma > 0.5$ (Figure 3a) and large Biot number, the product layer resistance dominates. As the reaction proceeds, a thicker product layer decreases the interfacial gaseous reactant concentration, $u_i$, but $u_i$ ultimately returns to unity as the reaction goes to completion and the interface $z$ vanishes. Hence, there is a minimum in $u_i$ during the course of the reaction, resulting in a maximum in $h(u_i)$ and consequently in $f_3(z)$. For lower $Bi$ values, the external mass-transfer resistance dominates, leading to relatively low $u_i$ values initially. However, since at reaction completion $u_i$ becomes unity, the $u_i$ value increases monotonically as reaction proceeds. Thus, $h(u_i)$ and $f_3(z)$ display monotonically increasing behavior, as seen in Figure 3a.

In Figure 3b for $\gamma < 0.5$, the uppermost and lower curves for large and relatively small Biot numbers are similar to those just discussed. For intermediate $Bi$ values (second curve from the top), *both* external film and product layer resistances must

be considered. The decreasing external mass-transfer resistance with shrinking particle dimension initially causes $u_i$ to increase. Subsequently, the developing product layer reverses this trend, but $u_i$ eventually returns to unity as the reaction goes to completion. These two reversals reflect in a minimum and a maximum in $f_3(z)$ as shown in Figure 3b.

### *Dynamics of reaction interface movement and preliminary shape considerations*

For monotone increasing kinetics $g'(u_i) \geq 0$, along with Eq. 14, Figures 2a, 3a, and 3b show the dynamics of the interface movement as well as its geometric stability. An accelerating reaction interface coordinate gives geometric instability, while a decelerating coordinate is stable (Doraiswamy and Sharma, 1984). Consider, for example, the case of a sphere ($F_p = 3$). As $z$ varies from 1 to 0, the corresponding value of the interface gas concentration, $u_i$, is obtained by the solution of Eq. 20: $h(u_i) = f_3(z)$. If the parameters $Bi$ and $\gamma$ lie in region I, as the reaction proceeds, $u_i$ increases monotonically from $u_{i,0}$, given by the unique solution of $h(u_i) = f_3(z) \equiv 1$, to $u_{if} = 1$, given by the unique solution of $h(u_i) = f_3(z) \equiv 0$. Then, from Eq. 14, the magnitude of the reaction front velocity $\dot{z}$ will also increase as the reaction proceeds. However, if $Bi$ and $\gamma$ lie in region II, $u_i$ first decreases from $u_{i,0}$ to its minimum value, $u_{im}$, and then increases eventually to 1 as $z$ decreases to 0, and the reaction front velocity will first decrease in magnitude and then increase continuously. Finally, region III corresponds to the case when $u_i$ first increases from $u_{i,0}$ to its maximum value, $u_{iM}$, decreases to its minimum value, $u_{im}$, and then increases eventually to 1 as $z$ decreases from 1 to 0. Hence, for $Bi$ and $\gamma$ pairs in region III, the reaction front speed will first increase to a local maximum, followed by a decrease to a local minimum, from which it will increase again to a final value.

It is worth noting that when dealing with particles of unchanging size ($\gamma = 1$), only regions I and II exist (Cao et al., 1993). The final value of $u_i$, that is, $u_{if} = 1$ for the case of spherical particles, while it is less than 1 for slab particles. This finding depends *only* on the shape of the particle itself. This can be explained by recalling that in the sphere case, as the surface area of the reacting interface decreases to zero, the concentration of the gaseous reactant at the interface continuously approaches the external value as the reaction goes to completion. On the other hand, the surface area of the reacting interface in the corresponding slab problem does not change with reaction and at the instant when the solid reactant is exhausted, the gas concentration remains finite and less than one. After this, there is nothing to sustain the gas concentration gradient within the product layer, and hence in due course it approaches unity.

For brevity, the case of cylindrical particles ($F_p = 2$) is not detailed since the behavior of $f_2(z)$ in Eq. 20 is similar to $f_3(z)$. Thus, an analogous behavior as in Figure 3c is obtained; particularly, the curve separating region I from region II is given by $Bi = \gamma^{-1}$. Also, $\gamma = 0.5$ again represents a critical number for this particle geometry. For $0 < \gamma < 0.5$, $f_2(z)$ reaches an inflection point at $\tilde{z} = [\gamma/(1-\gamma)]^{1/2}$. Thus, the locus of the points where $f_2'(\tilde{z}) = 0$, which separates regions I and III, is given by $Bi = 2[1 - \ln(2-2\gamma)]^{-1}$, which gives $Bi = 6.52$ at $\gamma = 0$ and $Bi = 2$ at $\gamma = 0.5$.

*For each particle geometry, these general considerations are independent of the form of the reaction kinetics $g(u_i)$, and depend solely on the relative magnitudes of the external and product diffusion resistances ($Bi$) and the ratio between the volume of solid product formed to the volume of the solid reactant ($\gamma$).* While the above analysis provides a qualitative picture of the reaction process, the different forms of $f_{F_p}(z)$ compared in the next section lead to the effects of particle shape.

## $f_{F_p}$ Inequalities from Particle Shape

Figures 2 and 3 show the interfacial dynamics for the slab and sphere geometries in general. A comparison of the functions $f_1$ and $f_3$ under equivalent conditions generates several fundamental inequalities on the interfacial concentration, the rate of advance of the reaction, and the time required to reach solid conversion that arise due to particle shape. These inequalities are valid for any nonlinear monotonically increasing kinetics $g(u_i)$, as well as for both expanding and shrinking particles.

We recall from Eqs. 21, 22 and 23 that $f$ functions are unity at $z = 1$ and note the inequalities of the slopes

$$f_1'(1) = 1 - \gamma(Bi+1) < 1 - \gamma(Bi-1) = f_3'(1). \tag{28}$$

The derivative $f_1'(1)$ is always less than unity (Figure 2a), combined with the nonvanishing property of $f_3''$ for $\gamma > 0.5$ (Figure 3a) guarantees that $f_1$ lies above $f_3$ for any $z$ and $\gamma$:

$$f_1 > f_3 \tag{29}$$

For $0 < \gamma < 0.5$, the inequality is restricted to sufficiently small values of $Bi$. To demonstrate this, let us examine the difference $(f_1 - f_3)$ from Eqs. 21 and 22:

$$f_1 - f_3 = (Bi-1)z(j-\lambda) \tag{30a}$$

where

$$j = \left(\frac{Bi\gamma + \gamma}{Bi - 1}\right)\left(\frac{1}{z} - 1\right) - 1 \tag{30b}$$

and

$$\lambda(z^{-1}) = -[(1-\gamma) + \gamma z^{-3}]^{-1/3}. \tag{30c}$$

In the case of $0 < Bi < 1$, $j < -1$ and $f_1$ will lie above $f_3$. In Figure 4, $j$ is plotted vs. $z^{-1}$ for various $Bi > 1$ and $\lambda$, and we seek the crossover value $\tilde{Bi}$ where $j$ is tangent to $\lambda$ coming from above. It is straightforward to show from Eq. 30c that for $0 < \gamma < 0.5$, $\lambda(z^{-1}) < 0$, $\lambda(1) = -1$, $\lambda' = d\lambda/d(z^{-1}) > 0$, $\lambda'(1) = \gamma$, and an inflection point $\lambda'' = d^2\lambda/d(z^{-1})^2 = 0$ occurs at $z^{-1} = \gamma^{-1} - 1$ where $\lambda''$ goes from positive to negative. The curve $\lambda$ is fixed in Figure 4 as $Bi$ is varied from unity, but the slope of $j$ decreases from a very large positive value for $Bi$ near unity down to its tangency with $\lambda$ at $\tilde{Bi}$, and then further down to its lowest value $\gamma$ when $Bi \to \infty$. For $Bi > \tilde{Bi}$, the region of crossover of $j$ and $\lambda$ generates an interval in $z^{-1}$ where $f_1 - f_3 < 0$. The $\tilde{Bi}$ in general, however, must be found numerically, as shown in Table 1. An analytical sufficient condition

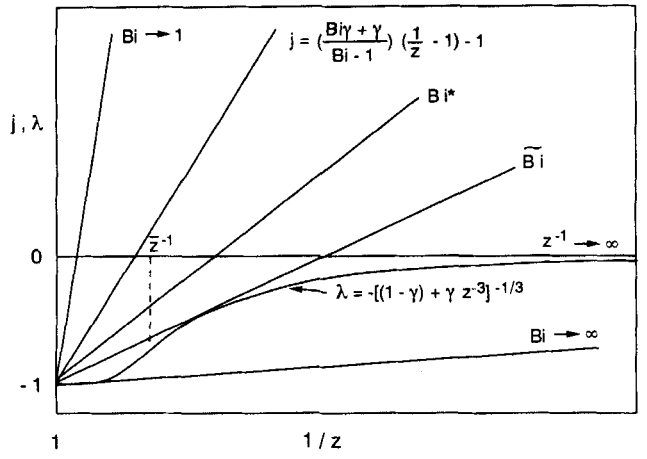


**Figure 4. Shape of functions $j$ and $\lambda$ given by Eqs. 30b and 30c for $0<\gamma<0.5$ and $Bi>1$.**

The straight lines represent the function $j$ for various values of $Bi$, while the sigmoidal curve represents the function $\lambda$. From Eq. 30a, the sign of the difference $f_1-f_3$ is the same as that of $j-\lambda$, and reverses sense for $Bi>\tilde{Bi}$ over an interval. For $Bi=Bi^*$, the slopes of $j$ and $\lambda$ at the inflection point $\bar{z}^{-1}$ are equal.

for the inequality can be obtained by setting $\lambda'(\overline{z^{-1}}) = j'(\overline{z^{-1}})$ and $\lambda''(z^{-1})=0$ at the inflection point:

$$Bi^* = (\chi+\gamma)/(\chi-\gamma) < \tilde{Bi} \tag{31a}$$

for

$$\chi = \gamma^{1/3}/[16(1-\gamma)^2]^{1/3} \tag{31b}$$

The condition $Bi<Bi^*$ is a sufficient condition for the shape inequality $f_1>f_3$. In general for $0<\gamma<0.5$, we have the less conservative exact condition

$$Bi<\tilde{Bi} \tag{32a}$$

for the pointwise inequality

$$f_1>f_3; \quad 0<\gamma<0.5. \tag{32b}$$

By following the same strategy as described above for spheres, $f_1$ and $f_2$ forms can also be compared. As the arguments are similar, we state only the results

$$f_1>f_2 \quad \text{for} \quad \gamma>0.5 \tag{33a}$$

**Table 1. Estimated Upper Limit on $Bi$ Values, $0<\gamma<0.5$***

| $\gamma$ | $\tilde{Bi}$ $(n=1)$ | $Bi^*$ $(n=1)$ | $\tilde{Bi}$ $(n=0)$ | $Bi^*$ $(n=0)$ |
|---|---|---|---|---|
| 0.05 | 2.32 | 1.99 | 14.80 | 11.37 |
| 0.1 | 3.69 | 3.05 | 15.80 | 12.27 |
| 0.15 | 5.61 | 4.53 | 18.67 | 14.53 |
| 0.2 | 8.52 | 6.77 | 23.55 | 18.31 |
| 0.3 | 22.18 | 17.23 | 46.88 | 36.16 |
| 0.4 | 96.38 | 73.49 | 167.88 | 127.87 |
| 0.5 | ∞ | ∞ | ∞ | ∞ |

* Pointwise inequalities $f_1-f_3>0$ and $\varphi_1-f_3>0$ continue to hold. $Bi^*$ is a weaker analytical estimate from Eq. 31a, while $\tilde{Bi}$ is a numerical determination.

and

$$f_1>f_2 \quad \text{for} \quad 0<\gamma<0.5 \quad \text{and} \quad Bi<\tilde{Bi} \tag{33b}$$

where $\tilde{Bi}$ is the tangency that occurs as the slope of the straight line $P=2(\text{Bi}\gamma+\gamma)Bi^{-1}(z^{-1}-1)$, decreasing with increasing $Bi$, contacts the curve $q=\ln[\gamma z^{-2}+1-\gamma]$. Similarly to the sphere case in Figure 4, equating the slope of the line $P$ with that of $q$, as well as setting $q''=0$ at its inflection point, gives an analytical lower bound on $\tilde{Bi}$ for a cylindrical particle

$$Bi^* = \gamma(\psi-\gamma)^{-1} < \tilde{Bi} \tag{33d}$$

with

$$\psi = \gamma^{1/2}/[2(1-\gamma)^{1/2}]. \tag{33e}$$

## Shape Inequalities on Interfacial Concentration, Reaction Coordinate, and Instantaneous Conversion

The fundamental shape inequalities for the slab vs. the sphere or the slab vs. the cylinder developed in the previous section hold for any monotone kinetics and any volume change $\gamma$ during reaction, with sufficient conditions subject only to an upper limit $Bi<\tilde{Bi}$ for $0<\gamma<0.5$. For fixed $Bi$, $\gamma$ and $Da$ values, the shape inequalities 29–32 for a sphere and 33 for a cylinder can be recast from Eq. 20 for any reaction coordinate value $z$ as:

$$(1-u_i)g^{-1}(u_i)\,|_{F_p=1} > (1-u_i)g^{-1}(u_i)\,|_{F_p=2,3} \tag{34}$$

For any specified monotone kinetics $g(u_i)$, this provides bounds for the interfacial concentration $u_i$ as

$$u_i|_{F_p=1} > u_i|_{F_p=2,3} \tag{35}$$

and from Eq. 14 leads directly to a shape bound on the interfacial rate of motion

$$0 \le -(dz/d\tau)\,|_{F_p=1} < -(dz/d\tau)\,|_{F_p=2,3}. \tag{36}$$

Integrating from unity to any $z$ provides the shape bounds on particle conversion times:

$$\tau|_{F_p=1} > \tau|_{F_p=2/3} \tag{37}$$

and conversely for the reaction position at any time $\tau$:

$$1 \ge z|_{F_p=1} > z|_{F_p=2,3} \ge 0. \tag{38}$$

Note that since $z$ is less than unity, as long as inequality 38 is valid, cubing $z$ for a sphere or squaring it for a cylinder to obtain the conversion $X$ from Eq. 19 will preserve the sense of the inequality at any time $\tau$:

$$0 \le X|_{F_p=2,3} < X|_{F_p=1} \le 1. \tag{39}$$

However, as a result, the shape inequalities on $X$ will be weaker than those on $z$.

**Table 2. First-Order Reaction $g(u)=u$: Dimensionless Time $\tau$ Required to Reach Reaction Interface Position $z$ for Particles of Changing Volume**

slab ($F_p=1$):

$$\tau_1 = 1 - z + \frac{Da}{2}\left[z^2 - 1 - \frac{\alpha^2 - 1}{1-\gamma} - \frac{2(\alpha^{n+1}-1)}{Bi(n+1)(1-\gamma)}\right]$$

cylinder ($F_p=2$):

$$\tau_2 = 1 - z + \frac{Da}{4}\left[1 + z^2(2\ln z - 1) - \frac{\alpha(\ln\alpha - 1)+1}{1-\gamma} + \frac{2(1-z^2)}{Bi}\right]$$

sphere ($F_p=3$):

$$\tau_3 = 1 - z + \frac{Da}{6}\left[3(1-z^2) + \frac{3(1-\alpha^{2/3})}{(1-\gamma)}\left(\frac{1}{Bi} - 1\right)\right]$$

To illustrate the shape bounds, we consider the slab, cylinder and sphere solutions in Table 2 for linear kinetics $g(u_i)=u_i$, for various $\gamma$, $Bi$ and $Da$ combinations. The case of slab with $n=0$ in the Appendix is also addressed here for comparison. As an example, let us consider the case $\gamma=2$ and $Bi=3$ lying in region II of Figure 3c. From Eqs. 29 and 33a, A5 and A11, both the $n=0$ and $n=1$ slab ($F_p=1$) solutions should bound from above the cylinder ($F_p=2$) and the sphere ($F_p=3$) plots for $z$, for all values of time $\tau$. However, since $\gamma>1$, the $n=0$ slab solution should be the best bound and in Figure 5a these $z$ shapes inequalities of Eq. A11 are clearly demonstrated. The weaker conversion inequalities of Eq. 39 and A20 are shown in Figure 5b.

The parameter values $\gamma=0.25$, $Bi=3$, and $Da=10$ lie in region I of Figure 3c. First, since $0<\gamma<0.5$, from Table 1, $Bi<Bi^*$ for both $n=0$ and $n=1$, hence inequalities 32b and A10 apply. For the cylinder, from Eqs. 33d and 33e, for $\gamma=0.25$ we have $Bi^*=25.8$ for $n=0$ and $\tilde{Bi}=12.9$ for $n=1$; since $Bi=3$ lies well below both of these, the slab shape inequality 33c can be used. However, since $\gamma<1$, the slab with $n=1$ should give the better shape inequality than $n=0$ as demonstrated in the Appendix. Figure 6a clearly shows this for $Da=10$, which is consistent with the corresponding $X$-shape inequalities in Figure 6b. Figures 5a and 6a also show that the sensitivity of $z$-shape curves to pellet geometry decreases as $\gamma$ decreases.

Outside $\gamma<0.5$ and $Bi>\tilde{Bi}$, shape inequalities A21-A26 and 34-39 apply without restriction for either $n=0$ or $n=1$. The case $\gamma=0.1$, $Bi=100$ and $Da=100$ is now selected, which lies within the space where sufficient conditions could not be established. While the inequality of the slab solutions, that is, the solution for $n=0$ lies above $n=1$ for $\gamma<1$, does not change following Eq. A2, Figure 7a clearly provides a counterexample for the shape inequalities. A complete inversion of the geometrical order is observed when comparing the $z$ plots of Figure 7a with those of Figures 5a and 6a. Thus, in general, for $0<\gamma<0.5$ and $Bi>\tilde{Bi}$, the $z$-shape inequality of slab over sphere and cylinder may not exist. Since all the $z$ values are between 0 and 1, in cubing $z$ for spheres or squaring $z$ for cylinders to calculate the conversion, a value of $z$ above the slab for a specific $\tau$ value may give a $z^3$ or $z^2$ that lies below the slab $z$. Clearly, the corresponding conversion curves in Figure 7b may not preserve the shape inequalities of Figure 7a.

## Application to Fluidized-Bed Reactor Design

Fluidized-bed reactors are employed for a variety of chemical and metallurgical processes (cf. Kunii and Levenspiel, 1969; Szekely et al., 1972), and in their modeling the noncatalytic reaction of particles with the surrounding fluid can frequently be described in terms of the SIM. In particular, by assuming uniform gas concentration, single size, mixed flow and no carryover of solids, it is well known (cf. Levenspiel, 1972) that the mean conversion of solids leaving the reactor can be written as:

$$\bar{X} = 1 - \int_0^{t|_{X=1}} (1-X)\frac{\exp(-t/\bar{t})}{\bar{t}}\,dt \qquad (40)$$

where $t|_{X=1}$ represents the time for complete reaction of a particle, $X$ is the solid conversion, and $\bar{t}$ is the mean residence time of solids in the reactor. For spherical particles ($F_p=3$) initially of uniform size, this expression which can be written in dimensionless form as

$$\bar{X}_{F_p=3} = 1 - \int_0^{t|_{X=1}} [1 - X_{F_p=3}(\tau)]\frac{\exp(-\tau/\theta)}{\theta}\,d\tau \qquad (41)$$

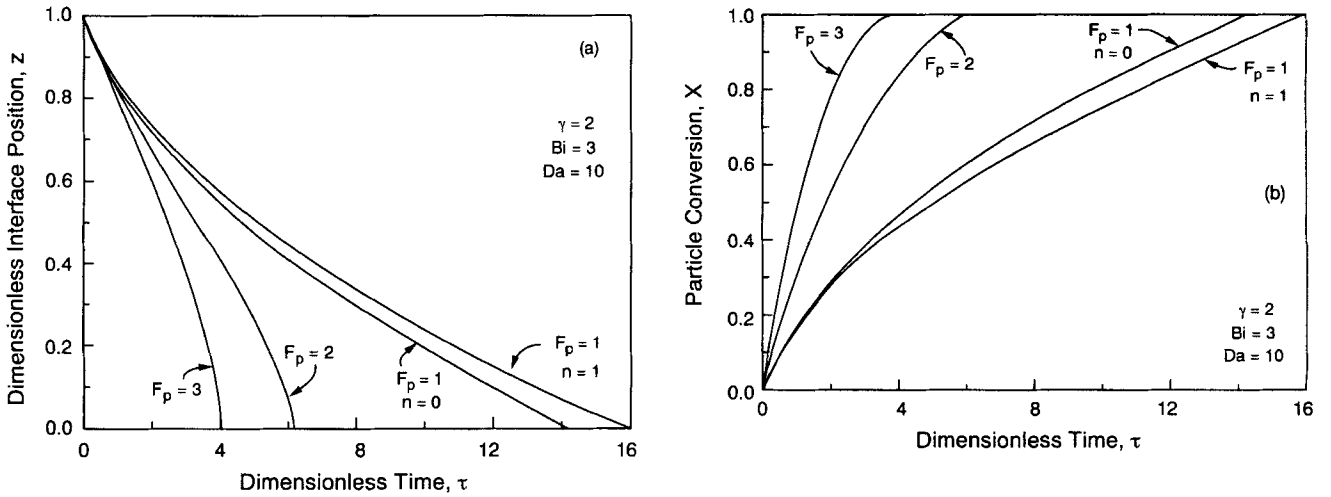


**Figure 5. General-shape inequalities for linear kinetics for $\gamma>1$.**

Slab results for $n=0$ are always closer to curves for the sphere and cylinder than $n=1$ for $\gamma>1$. The dimensionless interface position $z(a)$ and conversion $X(b)$ vs. dimensionless time $\tau$.

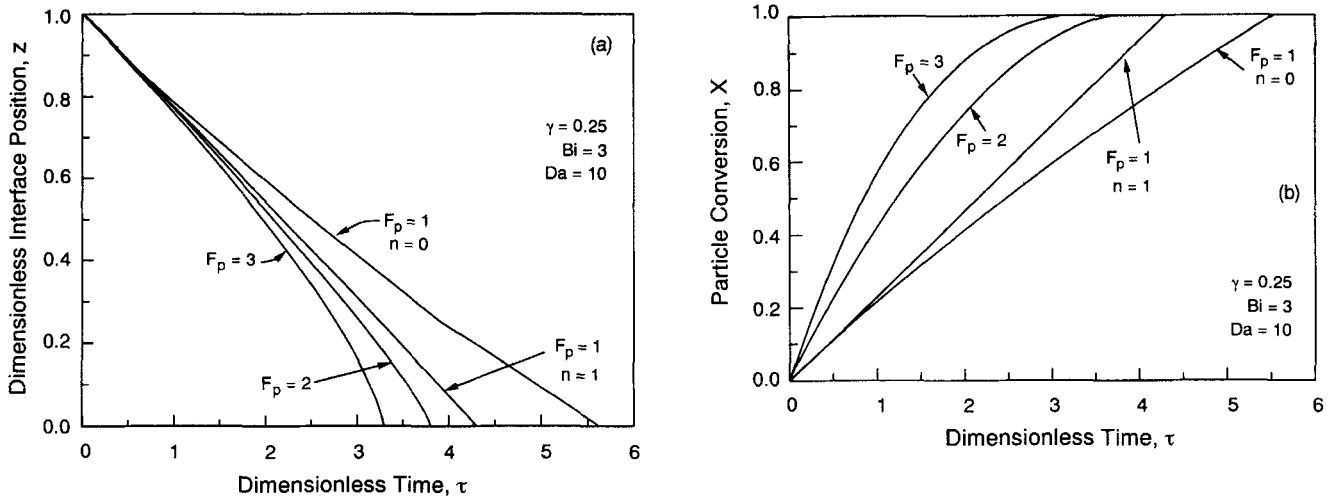


**Figure 6. General-shape inequalities for linear kinetics for $0.5<\gamma<1$ or $0<\gamma<0.5$ with $Bi<\tilde{Bi}$.**

Slab results for $n=1$ are always closer to curves for the sphere and cylinder than $n=0$ for $\gamma<1$. The dimensionless interface position $z(a)$ and conversion $X(b)$ vs. dimensionless time, $\tau$.

cannot be integrated analytically in general and has been evaluated in the literature *only* by assuming a particular controlling resistance as well as first-order reaction with respect to the gaseous reactant (cf. Yagi and Kunii, 1961; Levenspiel, 1962). Since the solid conversion is related to the dimensionless position of the reaction interface through Eq. 19, it follows from Eq. 38 that for *any* fixed set of $Da$, $g(u_i)$, $\gamma>0.5$ with any $Bi$ or $0<\gamma<0.5$ with $Bi<\tilde{Bi}$,

$$1-\overline{X}_{F_p=3}=\frac{1}{\theta}\int_0^{\tau_3} z^3_{F_p=3}(\tau)\exp(-\tau/\theta)d\tau$$

$$\leq\frac{1}{\theta}\int_0^{\tau_3} z^3_{F_p=1}(\tau)\exp(-\tau/\theta)d\tau$$

$$\leq\frac{1}{\theta}\int_0^{\tau_1} z_{F_p=1}(\tau)\exp(-\tau/\theta)d\tau \qquad (42)$$

where $\tau_{F_p}$ is the reaction time for complete conversion of the particle of geometry indicated by $F_p$. This result demonstrates that *the fraction of original solids of spherical shape which remains unconverted at the reactor exit is bounded above by the corresponding quantities related to particles of slab shape.* This is not surprising since in the last section we showed that, except for $\gamma<0.5$ and $Bi$ sufficiently large $Bi>\tilde{Bi}$, the solid conversion reached by a particle of spherical shape is always greater than the corresponding slab, and thus for the same residence time in a fluidized reactor this is also true for the mean solids conversion. In Eq. 42, while the extreme ends of the inequality demonstrate that the slab average conversion bounds that of the corresponding sphere (or cylinder for $F_p=2$), for practical purposes the middle $z^3_{F_p=1}$ integral will give better reactor volume estimates.

It is noted that the average conversion results can be applied for any nonlinear monotonic kinetics, and expanding or many cases of shrinking particles ($\gamma>0.5$) without restriction. If we specify the values of $\gamma$, $Da$, $Bi$ ($Bi<\tilde{Bi}$ for the case of $\gamma<0.5$) and consider linear kinetics, we find using $z_{F_p=1}(\tau)$ obtained for the case of first-order reaction with respect to the gaseous reactant, coupling Eqs. 14, 15, 20 and 21, the following explicit expressions of the integrals in inequality 42:

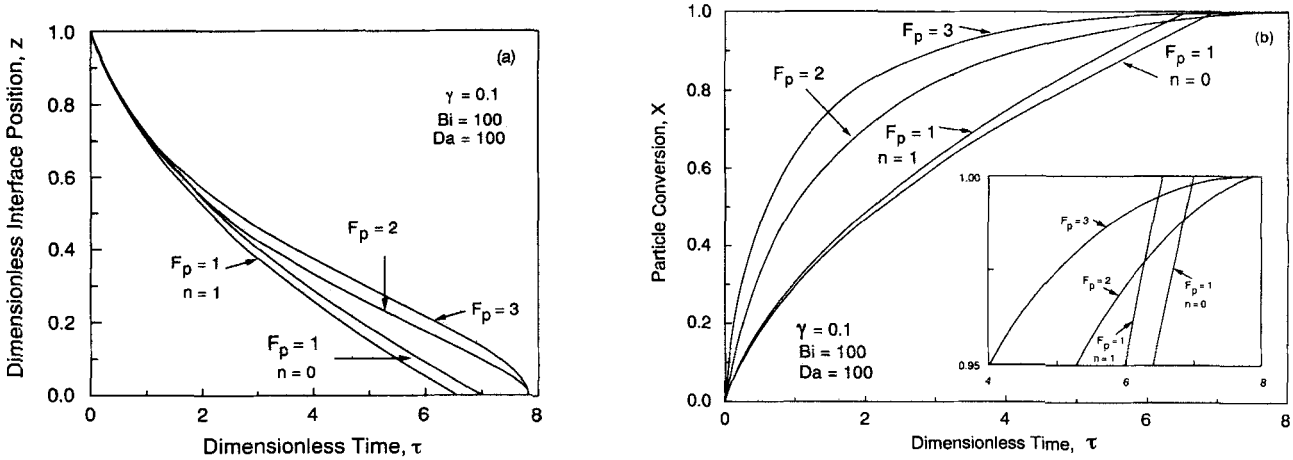


**Figure 7. Example of linear kinetics for $0<\gamma<0.5$ with $Bi>\tilde{Bi}$.**

In this region, shape inequalities can be violated. The dimensionless interface position $z(a)$ and conversion $X(b)$ vs. dimensionless time, $\tau$.

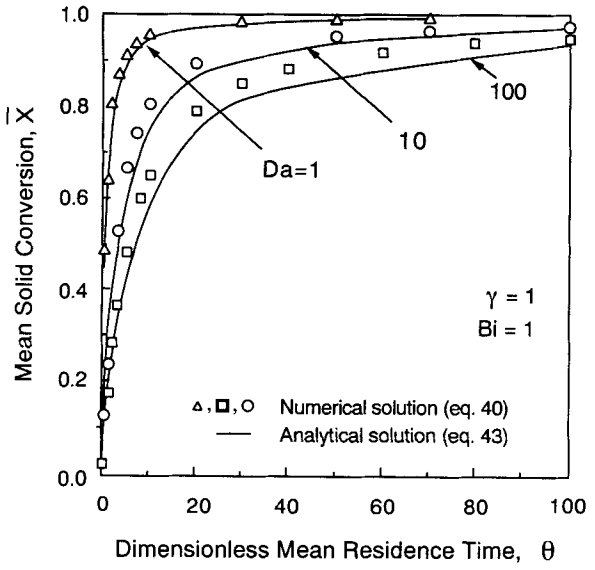


**Figure 8. Mean solid conversion $\bar{X}$ vs. dimensionless mean residence time $\theta$ for no volume change ($\gamma = 1$) and linear reaction kinetics.**

Circles are numerical solutions for spherical particles and solid lines are analytical lower bounds from Eq. 43.

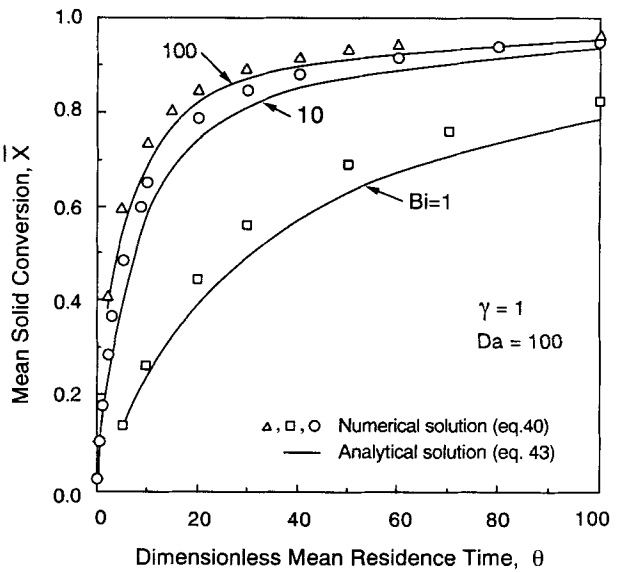


**Figure 9. Mean solid conversion $\bar{X}$ vs. dimensionless mean residence time $\theta$ for no volume change ($\gamma = 1$) and linear reaction kinetics.**

Circles are numerical solutions for spherical particles and solid lines are analytical lower bounds from Eq. 43.

$$\frac{1}{\theta}\int_0^{\tau_3} z^3_{F_p=1}(\tau)\exp(-\tau/\theta)d\tau$$

$$= [\exp(\mu_1)]\sum_{m=0}^{3}\frac{3!}{(3-m)!m!}a^m(1+a)^{3-m}\mu_1^{-m/2}\Gamma(1+m/2)$$

$$[\mu_2^{1+m/2}\gamma^*(1+m/2,\ \mu_2) - \mu_1^{1+m/2}\gamma^*(1+m/2,\ \mu_1)] \quad (43a)$$

where

$$a = (1+Bi\,Da^{-1})\,(Bi\,\gamma+\gamma^n-1)^{-1} \quad (43b)$$

$$\mu_1 = (1+Bi\,Da^{-1})\,(1+Da\,Bi^{-1})\,(Bi\,\gamma+\gamma^n-1)^{-1}(2\theta)^{-1} \quad (43c)$$

$$\mu_2 = \mu_1 + \tau_3\theta^{-1} \quad (43d)$$

$$\mu_2 = \mu_1 + \left[2 - Da - Da\frac{(1-\gamma^{2/3})}{(1-\gamma)}\left(\frac{1-Bi}{Bi}\right)\right](2\theta)^{-1} \quad (43e)$$

and $\gamma^*$ is the incomplete gamma function (Abramowitz and Stegun, 1964). Equation 43 represents an analytical lower bound on the average conversion in an isothermal fluidized-bed reactor with uniform gas concentration, single size, mixed flow and no carryover of solids considered to be of spherical shape. Equation 43 is derived *without any assumption about possible controlling regime, or about particle shrinkage or expansion.*

Figure 8 shows the mean conversion $\bar{X}$ of the solid as function of the dimensionless mean residence time $\theta$ for some combinations of *Da* and *Bi* values and for no volume change with reaction ($\gamma = 1$). The bound given by Eq. 43 is quite close to the true numerical solution of Eqs. 10, 14, 15, 18, 20 and 37 for spherical particles, where the latter was obtained using standard routines (IMSL Math/Library, 1989). For a fixed value of the Damköhler number *Da*, the accuracy of the bound given by Eq. 43 increases with increasing values of *Bi*. As *Bi* increases, that is, the mass-transfer resistance in the external film around the particles decreases, higher values of the mean solid conversion are reached for a fixed value of the mean residence time. Figure 9 shows similar behavior in terms of accuracy of the bound given by Eq. 43 with respect to the true numerical solution, when decreasing the value of the Damköhler number for a fixed value of *Bi*. Note that for a fixed conversion, the dimensionless mean residence time $\theta$ increases with increasing *Da*. This seeming anomaly occurs because $\theta$ is itself proportional to *Da* (cf. Ramachandran, 1982). The analytical bound Eq. 43 on the mean conversion includes the possibility of size change and in Figures 10a-10b the bounds are plotted for $\gamma = 2$ and $\gamma = 0.5$, respectively, for $Da = 100$ and $Bi = 10$, and can be compared with the midcurve in Figure 8 for $\gamma = 1$. As expected, conversion decreases with increasing $\gamma$.

In the investigated region of parameter values, the solution of the integral 43 for $n = 0$ provides values that are only a few percent different from the $n = 1$ solution. In particular, the integral 43 for $n = 1$ provides the better bound for $\gamma < 1$, while $n = 0$ provides the better bound for $\gamma > 1$ and the bounds crossover for a constant volume reaction $\gamma = 1$. For most practical applications, the two bounds (with $n = 0$ and 1) from Eq. 43 are quite close and only for values of $\gamma$ which are outside physical limits ($\gamma > 9$), the difference between the two solutions becomes significant.

Finally, we note that owing to its accuracy in reproducing the true numerical solutions, the bound given by Eq. 43 can be used conveniently for reactor design. For any mean solids conversion, the required residence time evaluated through this bound and hence the reactor volume guarantees the desired mean conversion of solids of spherical shape, as shown in Figures 8, 9, and 10.

## Concluding Remarks

Fundamental aspects of diffusion-reaction interaction for

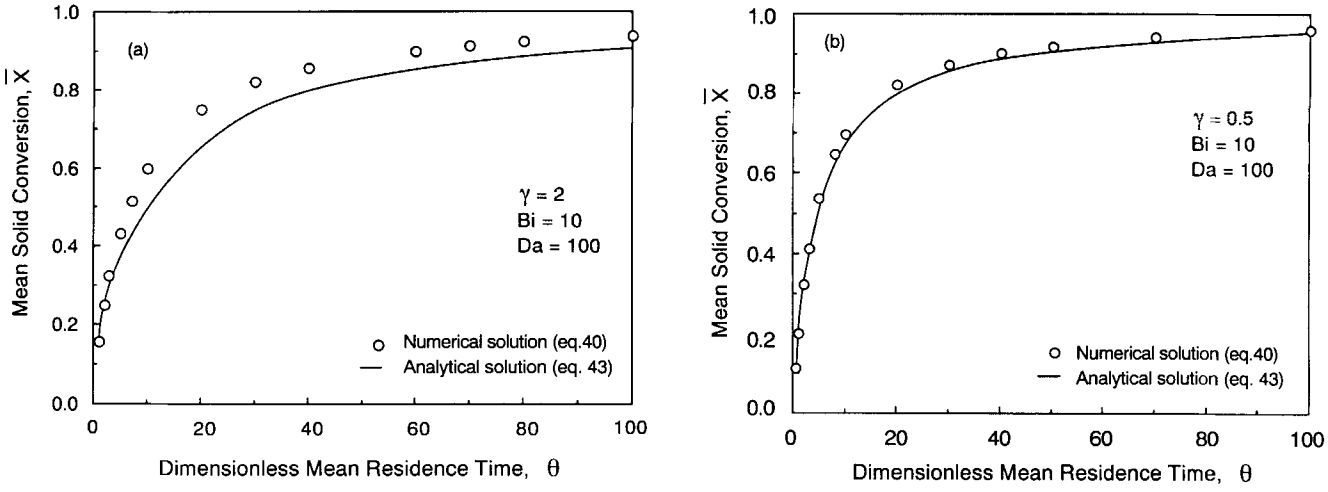


**Figure 10. Mean solid conversion $\bar{X}$ vs. dimensionless mean residence time $\theta$ for linear reaction kinetics.**

Circles are numerical solutions for spherical particles and solid lines are analytical lower bounds from Eq. 43 from the slab shape analysis. For expanding particles ($\gamma = 2$) $n = 0$ is the better bound, while for shrinking particles ($\gamma = 0.5$) $n = 1$ gives the tighter lower bound.

nonlinear gas-solid reactions following the sharp interface model, uncovered here for the first time, are as follows.

- Depending on the relative magnitudes of the external mass transfer ($Bi$), the ratio of the volume of the reaction products to that of the starting materials ($\gamma$), and the particle shape ($F_p$), the dimensionless gaseous reactant concentration at the reaction interface of a spherical or cylindrical particle ($u_i$) may exhibit different features. Starting from a certain initial value related to the above mentioned parameters: a) for small $Bi$, it increases monotonically to unity as the solid reactant is consumed; b) for large $Bi$, it first decreases to a minimum as the product layer resistance builds up, and then increases to unity at the cessation of the reaction; and c) for shrinking particles and intermediate $Bi$, it first increases to a maximum, decreases to a minimum, and then increases to unity at the cessation of the reaction. For the slab shape, the behavior is simpler; there is either a monotone increase of a monotone decrease from the initial to the final value.
- While this study is limited to the isothermal problem as noted by Mazet (1992), this assumption is valid for the majority of cases. Any arbitrary monotone nonlinear kinetics, volume change, and mixture of rate controlling steps are considered. A systematic analysis of the evolution of the reaction in the parameter space allows us to establish rigorously the effect of particle shape. The solid conversion reached by a particle of spherical or cylindrical shape is always greater than that of a slab particle for all $Da$, $\gamma$, and $Bi$ ($Bi < \tilde{Bi}$ for $0 < \gamma < 0.5$). Similar inequalities exist for the interfacial concentration, reaction coordinate, and speed of the reaction front.
- For a fluidized-bed reactor containing solid particles of spherical shape, the fractional conversion of solid cannot be obtained analytically in general, even for a first-order reaction. By taking advantage of the *a-priori* bounds, however, the unconverted fraction at the reactor exit is bounded by the corresponding values related to particles of slab shape. In particular, one of these bounds can be obtained analytically for a first-order reaction with respect to the gaseous reactant, without any approximation about possible controlling regimes.

In examples involving linear kinetics, various $Da$ and $Bi$ values, and fixed volume, expanding or shrinking particles, these analytical expressions give excellent accuracy when compared with exact numerical solutions and hence can be used conveniently for reactor design. The accuracy of these linear kinetics bounds and the analytical pointwise bounds of Cao et al. (1993) for nonlinear kinetics suggests that expressions similar to Eq. 43 can be obtained for changing particle size with nonlinear kinetics as well.

## Acknowledgments

We gratefully acknowledge the fellowship awarded to G. C. by the Consiglio Nazionale delle Ricerche (CNR), Rome, Italy. Acknowledgment is also made to the Donors of the Petroleum Research Fund, administered by the American Chemical Society, for partial support of this research.

## Notation

$Bi$ = Biot number, $k_{g0}R_0/D_e$
$\tilde{Bi}$ = value of $Bi$ when $j$ (or $P$) is tangent to the curve $\lambda$ (or $q$)
$Bi^*$ = a bound for $\tilde{Bi}$
$C$ = concentration
$D_e$ = effective diffusivity of component $A$
$Da$ = Damköhler number, $R_0 f(C_{Ab})/D_e C_{Ab}$
$f(C_{Ai})$ = interface reaction kinetics
$f_{F_p}(z)$ = function defined by Eq. 20
$g(u_i)$ = dimensionless interface reaction kinetics
$h$ = function defined by Eq. 20
$F_p$ = shape factor
$k_{g0}$ = gas-film mass-transfer coefficient for constant particle size
$j$ = quantity defined by Eq. 30b
$M$ = molecular weight
$n$ = parameter in Eq. 2 which depends on the particle Reynolds number
$q$ = function defined by Eqs. 16–18
$R$ = characteristic length for any particle shape at any time
$R_A$ = interface reaction rate
$R_i$ = position of the reaction interface
$S_p$ = particle surface area
$t$ = time
$\bar{t}$ = mean residence time

$u$ = dimensionless gas concentration, $C_A/C_{Ab}$
$V_p$ = particle volume
$X$ = solid conversion
$\overline{X}$ = mean conversion of solids leaving the reactor
$z$ = dimensionless position of the reaction interface, $R_i/R_0$
$z^{-1}$ = value at which $\lambda(z^{-1})$ [or $q(z^{-1})$] has an inflection point

### Greek letters

$\alpha$ = $\gamma+(1-\gamma)z^{F_p}$
$\gamma$ = volume of product $S$ formed per unit volume of reactant $B$ reacted, $\rho_B\nu_S M_S/\rho_S\nu_B M_B$
$\lambda$ = function defined by Eq. 30c
$\varphi_1$ = function defined by Eq. A1
$\zeta$ = function defined by Eq. A8
$\theta$ = dimensionless mean residence time, $\nu_B f(C_{Ab})M_b\bar{t}/\nu_A\rho_B R_0$
$\nu$ = stoichiometric coefficient
$\rho$ = density
$\tau$ = dimensionless time, $\nu_B f(C_{Ab})M_B t/\nu_A\rho_B R_0$
$\tau_{F_p}$ = dimensionless time required for conversion $X=1$ for particles of different shape
$\chi$ = quantity defined by Eq. 31b
$\psi$ = quantity defined by Eq. 33e
$\psi_A$ = dimensionless interface reaction rate, $R_A/R_{Ab}$

### Subscripts

$A$ = gas reactant
$b$ = value in the bulk of the gas phase
$B$ = solid reactant
$f$ = final value
$i$ = value at the interface between the product layer and the unreacted core
$m$ = minimum value
$M$ = maximum value
0 = initial value
$P$ = gas product
$s$ = value at the particle external surface
$S$ = solid product

## Literature Cited


Abramowitz, M., and I. A. Stegun, *Handbook of Mathematical Functions*, Nat. Bur. of Std., Washington, DC (1964).

Baron, R. E., J. L. Hodges, and A. F. Sarofim, "Mathematical Model for Predicting Efficiency of Fluidized Bed Steam Generators," *AIChE Symp. Ser.*, **74**(176), 120 (1978).

Cao, G., A. Varma, and W. Strieder, "Approximate Solutions for Nonlinear Gas-Solid Noncatalytic Reactions," *AIChE J.*, **39**, 913 (1993).

Carberry, J. J., *Chemical and Catalytic Reaction Engineering*, McGraw-Hill, New York (1976).

Doraiswamy, L. K., and M. M. Sharma, *Heterogeneous Reactions: Analysis, Examples, and Reactor Design*, Wiley, New York (1984).

Geldart, D., ed., *Gas Fluidization Technology*, Wiley, Chichester (1986).

*IMSL Math/Library*, FORTRAN Subroutines for Mathematical Applications (1989).

Levenspiel, O., *Chemical Reaction Engineering*, 2nd ed., Wiley, New York (1972).

Kunii, D., and O. Levenspiel, *Fluidization Engineering*, Wiley, New York (1969).

Mazet, N., "Modeling of Gas-Solid Reactions: 1. Nonporous Solids," *Int. Chem. Eng.*, **32**(2), 271 (1992).

Ramachandran, P. A., "Analysis of Non-Catalytic Reactions Following Langmuir-Hinshelwood Kinetics," *Chem. Eng. J.*, **23**, 223 (1982).

Szekely, J., J. W. Evans, and H. Y. Sohn, *Gas-Solid Reactions*, Academic Press, New York (1972).

Yagi, S., and D. Kunii, "Fluidized-Solids Reactors with Continuous Solids Feed: II," *Chem. Eng. Sci.*, **16**, 372 (1961).

Yoshida, K., and C. Y. Wen, "Noncatalytic Solid-Gas Reaction in a Fluidized Bed Reactor," *Chem. Eng. Sci.*, **25**, 1395 (1970).


## Appendix

The results obtained when considering the case of constant film resistance, $n=0$, for the flat plate are summarized here and compared with those for other geometries when $n=1$. From Eq. 20, we have:

$$\varphi_1 = Bi\gamma + 1 - Bi\gamma z = h(u_i) \tag{A1}$$

which represents the dashed straight line in Figure 2a, whose slope is $\varphi_1' = -Bi\gamma$. The two functions $f_1$ and $\varphi_1$ are identical for $\gamma=1$. For the shrinking particle ($\gamma<1$), all three cases of $f_1$ in Figure 2a lie below the line for $\varphi_1$,

$$\varphi_1 > f_1 \quad \text{for} \quad \gamma<1. \tag{A2}$$

For the expanding particle ($\gamma>1$), both cases ($n=0$, 1) allow only increasing $\varphi_1$ and $f_1$ functions as $z$ decreases from 1 to 0, that is, decreasing $u_i$, and the uppermost line $f_1$ for $\gamma>1$ always lies above $\varphi_1$:

$$\varphi_1 < f_1 \quad \text{for} \quad \gamma>1. \tag{A3}$$

For $n=0$, region II in Figure 2b is the entire $Bi$-$\gamma$ plane. From Eqs. 20 and A1

$$\varphi_1'(1) = -Bi\gamma < 1-\gamma(Bi-1) = f_3'(1). \tag{A4}$$

Using the same arguments utilized in the text and considering Eqs. A2 and A3 we have

$$f_1 > \varphi_1 > f_3 \quad \text{for} \quad \gamma>1 \tag{A5}$$

and

$$\varphi_1 > f_1 > f_3 \quad \text{for} \quad 1>\gamma>\frac{1}{2}. \tag{A6}$$

The tighter inequalities give the best shape bounds as discussed earlier. For $0<\gamma<0.5$, the same strategy followed for $(f_1-f_3)$ is considered when analyzing the difference $(\varphi_1-f_3)$. From Eqs. A1 and 22

$$\varphi_1 - f_3 = (Bi-1)z(\zeta-\lambda), \tag{A7}$$

where

$$\zeta = \left(\frac{Bi\gamma+1}{Bi-1}\right)\left(\frac{1}{z}-1\right)-1 \tag{A8}$$

and $\lambda(z^{-1})$ is defined in Eq. 30c. A plot similar to that in Figure 4 can be constructed. The inequality $Bi<Bi^*<\tilde{Bi}$, where $Bi^*$ is given by

$$Bi^* = (\chi+1)/(\chi-\gamma) < \tilde{Bi} \tag{A9}$$

with $\chi$ as in Eq. 31b represents a sufficient condition for

$$\varphi_1 > f_1 > f_3; \quad 0 < \gamma < 0.5 \tag{A10}$$

Since for $0<\gamma<0.5$, $j<\zeta$ for any finite $Bi$, the critical $\tilde{B}i$ and $Bi^*$ for $n=0$ lie above those for $n=1$ (Table 1). As each bound $\varphi_1$ and $f_1$ applies independent of the other, $\tilde{B}i$ for $n=1$ relates to $f_1$; however, above that $Bi$ value the $\varphi_1$ inequality will continue to apply until $\tilde{B}i$ for $n=0$ is reached. The weaker bound gives broader coverage.

By following the same strategy as described earlier, the $\varphi_1$ and $f_2$ forms can also be compared. As the arguments are similar, we state only the results in this case:

$$f_1 > \varphi_1 > f_2 \quad \text{for} \quad 1 < \gamma, \tag{A11}$$

$$\varphi_1 > f_1 > f_2 \quad \text{for} \quad 0.5 < \gamma < 1, \tag{A12}$$

$$\varphi_1 > f_1 > f_2 \quad \text{for} \quad 0 < \gamma < 0.5 \tag{A13}$$

whenever

$$Bi < \tilde{B}i,$$

where $\tilde{B}i$ is the tangency that occurs as the slope of the straight line $\Omega = 2(Bi\gamma + 1)Bi^{-1}(z^{-1}-1)$, decreasing with increasing $Bi$, contacts the curve $q$. An analytical lower bound on $\tilde{B}i$ for a cylindrical particle is

$$Bi^* = (\psi - \gamma)^{-1} < \tilde{B}i, \tag{A14}$$

with $\psi$ given by Eq. 33e.

From the fundamental shape inequalities above, the following inequalities on the interfacial concentration, reaction coordinate and instantaneous conversion can be obtained for $\gamma > 1$:

$$(1-u_i)g^{-1}(u_i)|_{F_p=1,n=1} > (1-u_i)g^{-1}(u_i)|_{F_p=1,n=0} > (1-u_i)g^{-1}(u_i)|_{F_p=2,3} \tag{A15}$$

$$u_i|_{F_p=1,n=1} > u_i|_{F_p=1,n=0} > u_i|_{F_p=2,3} \tag{A16}$$

$$0 \le -(dz/d\tau)|_{F_p=1,n=1} < -(dz/d\tau)|_{F_p=1,n=0} < -(dz/d\tau)|_{F_p=2,3} \tag{A17}$$

$$\tau|_{F_p=1,n=1} > \tau|_{F_p=1,n=0} > \tau|_{F_p=2,3} \tag{A18}$$

$$1 \ge z|_{F_p=1,n=1} > z|_{F_p=1,n=0} > z|_{F_p=2,3} \ge 0 \tag{A19}$$

$$0 \le X|_{F_p=1,n=1} > X|_{F_p=1,n=0} > X|_{F_p=2,3} \le 1 \tag{A20}$$

and for $0.5<\gamma<1$, as well as for $0<\gamma<0.5$ whenever $Bi<\tilde{B}i$:

$$(1-u_i)g^{-1}(u_i)|_{F_p=1,n=0} > (1-u_i)g^{-1}(u_i)|_{F_p=1,n=1} > (1-u_i)g^{-1}(u_i)|_{F_p=2,3} \tag{A21}$$

$$u_i|_{F_p=1,n=0} > u_i|_{F_p=1,n=1} > u_i|_{F_p=2,3} \tag{A22}$$

$$0 \le -(dz/d\tau)|_{F_p=1,n=0} < -(dz/d\tau)|_{F_p=1,n=1} < -(dz/d\tau)|_{F_p=2,3} \tag{A23}$$

$$\tau|_{F_p=1,n=0} > \tau|_{F_p=1,n=1} > \tau|_{F_p=2,3} \tag{A24}$$

$$1 \ge z|_{F_p=1,n=0} > z|_{F_p=1,n=1} > z|_{F_p=2,3} \ge 0 \tag{A25}$$

$$0 \le X|_{F_p=1,n=0} > X|_{F_p=1,n=1} > X|_{F_p=2,3} \le 1 \tag{A26}$$

The shape inequalities above are compared in Figures 4-6 for selected combinations of the parameter values.

*Manuscript received Dec. 22, 1993, and revision received Mar. 30, 1994.*